



Mania, R. J., and York, C. B. (2017) Buckling strength improvements for Fibre Metal Laminates using thin-ply tailoring. *Composite Structures*, 159, pp. 424-432. (doi:10.1016/j.compstruct.2016.09.097)

There may be differences between this version and the published version. You are advised to consult the publisher's version if you wish to cite from it.

<http://eprints.gla.ac.uk/129415/>

Deposited on: 10 October 2016

Enlighten – Research publications by members of the University of Glasgow
<http://eprints.gla.ac.uk>

Buckling strength improvements for Fibre Metal Laminates using thin-ply tailoring

Radosław Mania*

Department of Strength of Materials Lodz University of Technology Stefanowskiego
1/15, 90-924 Lodz, PL

Christopher Bronn York†

Department of Mechatronics and Mechanical Systems Engineering, University of São
Paulo, Av. Professor Mello Moraes, 2231, São Paulo, SP, 05508-030, Brazil.

Abstract

The buckling response and load carrying capacity of thin-walled open cross-section profiles made of Fiber Metal Laminates, subjected to static axial compression loading are considered. These include thin-walled Z-shape and channel cross-section profiles adopting a 3/2 FML lay-up design, made of 3 aluminium layers. The objective of the investigation is the comparison of standard thickness Fibre Reinforced Plastic layers

*Corresponding author: Tel: +48 42 631 22 21, E-mail address:

Radoslaw.Mania@p.lodz.pl

†Permanent address: Aerospace Sciences, School of Engineering, University of
Glasgow, University Avenue, G12 8QQ, Glasgow, Scotland.

versus thin-ply material technology. Whilst thin ply designs differ only by the layer thickness, they offer an exponential increase in stacking sequence design freedoms, allowing detrimental coupling effects to be eliminated. The benefit of different hybrid materials are also considered. The comparisons involve semi-analytical and finite element methods, which are validated against experimental investigations.

Keywords

Bending-Twisting coupling; Compression Buckling; Non-dimensional Stiffness Parameters; Lamination Parameters; Fibre Metal Laminates; Thin Ply Material

1. Introduction

The past few decades have seen the introduction of Fiber Metal Laminates (FMLs), especially GLARETM, into primary structure applications such as the fuselage of the largest civil transport aircraft in current production: the Airbus A380. GLARETM material properties, as well as FMLs in general, exhibit partly metallic and partly composite behaviour. The hybrid nature of FMLs has the advantage of lower density when compared with monolithic aluminium fuselage skins, but more importantly it has natural crack arresting capability due to the fibre layers in the presence of a fatigue crack, which is a major concern in the design of monolithic aluminium [1]. These features reduce the concerns about 'flying with undetectable fatigue damage', which influences inspection intervals and the economics of airframe maintenance [2]. However, the hybridization of materials in multi-layered structures leads inevitably to a decrease in the buckling load capacity, which is only partly off-set by a weight reduction.

Multi-layered Fibre Reinforced Plastic (*FRP*) materials are very effective for meeting tailored structural property requirements through appropriate modification of the material stiffness, which governs the laminate response. Controlling the bending stiffness, for instance, through appropriate stacking sequence tailoring, material and ply thickness selection, has the potential to give improvements in the compressive buckling load capacity for FML, as will be demonstrated for short columns of open cross-section.

The advantages of FMLs results from their architecture, which typically contains layers of unidirectional Glass Fibre-Reinforced Plastic (GFRP) material embedded between thin aluminium sheets. Various properties can be achieved using different grades of commercially available FML, e.g., GLARETM, which have been developed for specific structural applications [3].-However, the merits of FMLs are most often exploited in weight saving applications associated with thin-walled design of aircraft structures, which are generally subject to high in-plane stresses. Instability phenomena therefore become one of the most important design constraints and need to be satisfied for safety reasons [4].

Research on FML structures has focused primarily on the main advantages over monolithic aluminium alloys: increased fatigue life, reduced crack propagation rates and corrosion resistance [1]. The first FMLs used aramid fibres, but were soon replaced by glass fibres. Other hybrids were also considered, such as carbon/epoxy composite, polyamide and titanium. Although, the dominant material still consists of laminated GFRP with aluminium alloys [5, 6] due primarily to its resistance to galvanic corrosion.

The use of FML in stiffened fuselage skin panels with monolithic aluminium stringers lead to issues related to stiffness mismatching, since the higher elastic modulus of the

aluminium stringers attracts more load from the skin panels, which creates fatigue problems in the stringers. FML stringers have therefore been developed [8] to alleviate these issues. These are most commonly manufactured by wet lay-up of the complete GFRP sub-laminate, pre-forming the FML and then curing. The stiffener is either bonded to the skin with a polymer adhesive, or by a fibre reinforced polymer interface with reduced fibre volume fraction. The stiffeners must therefore resist out of plane loading as well as in-plane compressive loading.

The objective of current article is to demonstrate improvements the compression buckling strength of typical thin-walled profiles through the use of different hybrid FML strategies and by the introduction of thin-ply material technology. The profiles are treated in isolation, i.e. open cross-sections made of FML materials, thus removing any stabilizing influence of the skin [6].

Thin-ply composite materials are now commercially available, in a range of areal weights [7]. Compared to composite materials with standard areal weight of approximately 250 g/m^2 , thin-ply laminates, with areal weights down to as little 15 g/m^2 , generate lower interface stresses, which significantly improves key mechanical properties such as ultimate strength, strength after impact due, to improved delamination resistance, and better control of crack propagation due to the increased number of ply angle interfaces through the thickness [10]. Thin-plies extend the design space by increasing the number of possible ply combinations within a given thickness, thus improving the chances of obtaining an optimal stacking sequence. New hybrid lamination schemes are introduced in which conventional plies are replaced by thin-ply sub-laminates.

2. Subject of investigations

Buckling assessments of thin-walled Fibre Metal Laminate (FML) profiles, of Z- and Channel-shape cross section, are obtained using semi-analytical and numerical methods and validated experimentally. Both cross-section types represent short columns with matching flange and web dimensions. The width of the web was equal to 80 mm, flange to 40 mm, with a profile length of 300 mm. The corner radius (R) at the web/flange junction is approximately equal to 1.75 mm, as shown in Fig. 1 (a) and (b).

The column specimens were manufactured by wet lay-up of the FML and cured under a standard autoclave cycle [11]. Some specific information and manufacturing procedures applied to the FML specimens are discussed elsewhere [6]. All manufactured specimens were of 3/2 type FML, i.e., a 7-layer hybrid laminate containing alternating layers of aluminium and angle- or cross-ply pairs of fibre-reinforced composite layers. The Aluminium was a 2024 T3 alloy with thickness of a single layer equal to 0.3mm, whereas glass/epoxy uni-directional (UD) fibre-reinforced plastic (TVR 380 M12 26% R-glass, from Hexcel), with a 60% fibre volume fraction, had a single layer thickness, after curing, equal to 0.25 mm. The test specimens contained pairs of adjacent GFRP layers, see Fig. 2, and only symmetrical lay-ups were considered.

Table 1 presents the various FML stacking sequences considered in the buckling and post-buckling analyses. Only the first seven lay-ups were manufactured and tested in the laboratory. Among these, sequences representing standard GLARE™ grades are identified, as: FML 1 - GLARE 3; FML 5 - GLARE 2A and; FML 10 - GLARE 6A. FML 6 and 7 contain shallow angle sub-laminates for comparison in future design studies. They contain designs matching current trends in non-crimp fabric development.

FML 8 represents a monolithic aluminium profile, providing a datum configuration against which all other designs can be compared. An alternative datum is represented by FML 9, containing composite layers with fully isotropic properties [12].

The mechanical properties for aluminium are given in Table 2, and those of glass-epoxy from TVR Hexcel composites are given in Table 3. Due to discrepancies observed during the buckling experiments [6], these properties were measured in laboratory tests [13], and led to an improvement in the agreement between experiment and semi-analytical and numerical results; in comparison to the data provided by the material supplier.

3. Buckling response of analysed column/profile

Two simulation methodologies were employed for examination of the buckling response of short FML column profiles. These were: a semi-analytical method based on Koiter's asymptotic theory of conservative systems [14] and; the finite element method [15]. These simulations were verified experimentally [6, 16]. For the simulations, it was assumed that the loaded edges of the axially compressed columns were simply supported. Such boundary conditions are easy to apply in a semi-analytical solution, but for the numerical approach, the FEM model of Fig. 3(b) adopted with shell finite elements, and required careful selection of the constraints at the loaded edges of each profile. It is also difficult to achieve boundary conditions that precisely match these simply supported edge conditions in experimental tests [17, 18]. Nevertheless, in current study the loading platens (upper and lower) were designed to reproduce the idealized analytical and numerical boundary conditions very closely. Shallow grooves, equivalent to the profile wall thickness, H , in depth, with a flat bottom and 45°

chamfered edges, were milled into both platens; the width of the grooves provided a clearance of $0.1H$ was to accommodate variations in the profile wall thickness. Thick upper and lower platens ensured uniform compression of the profiles, see Fig. 3(a).

A Digital Image Correlation technique was employed to detect the onset of buckling. This is a 3D non-contact optical measurement system of full field surface deformations, see Fig. 3(c). Full details of the procedure for the buckling experiments, and methods of data capture and processing, can be found elsewhere [6, 16, 18]; only the results are discussed here. The resulting images of the buckling modes confirmed both the semi-analytical and numerical predictions.

4. Comparison of buckling load

The discussion henceforth is restricted to the results obtained for the channel section profile. Discussion of the results for the Z-shaped profile can be found elsewhere [6, 13, 15, 16]. Table 4 summarises the buckling load results for the experiment, FEM and semi-analytical methods. Not all manufactured FML specimens were included in laboratory test program hence a number of rows in the table have missing results. The last three lay-ups were not tested, but provide benchmarks against which the other configurations may be meaningfully compared, i.e., monolithic aluminium, an FML with isotropic *FRP* sub-laminates and GLARE 6A.

Table 4 reveals good agreement between the buckling loads determined from laboratory experiments and Finite Element computations. However, buckling loads predictions using the semi-analytical (Koiter) method are lower than the others due to neglecting the corner radius at the web/flange joints. This simplified modelling lowers the stiffness

of the column and hence it's buckling load. When compared to the experimental results, the differences in buckling load vary by up to 11%, whereas the variation between the first two methods does not exceed 4%.

If the buckling load of a particular FML profile is compared to that of the monolithic aluminium section, there is a pronounced reduction in buckling load. For the $[Al/90/0/Al/0/90/Al]_T$ cross-ply stacking sequence, this reduction is as high as 26%, compared to approximately 22% for the $[Al/45/-45/Al/-45/45/Al]_T$ angle-ply FML profile. The source of this degradation in buckling load can be attributed to the difference between Young's moduli of aluminium and glass-epoxy sub-laminate. The different sub-laminate configurations appear to have relatively little influence on the buckling of the FML.

Figure 4 compares the load-deflection behaviour of channel sections with FML designs 1, 3, and 5, listed in Table 1. Here, nonlinear buckling FEM analysis predictions are compared to the experimental results. In the post-buckling range, above 30kN, the equilibrium paths of the three designs have similar stiffness gradients, but toward the middle of the post-buckling range, above 40kN, the gradients differ substantially. FML 5 or GLARE 2A has the highest gradient due to the axially stiff sub-laminate, i.e. $[Al/0/0/Al/0/0/Al]_T$. By contrast FML 1, or GLARE 3, has the lowest gradient and the weakest axial stiffness of the three sub-laminates, i.e. $[Al/0/90/Al/90/0/Al]_T$. However, this relationship does not follow directly from observations of the initial buckling response, determined both experimentally and through Eigenvalue-buckling analysis. FML 3 exhibits the highest static buckling load among the three designs whereas it's post-buckling stiffness drops in comparison to the others. The sub-laminate of FML 3 is

un-balanced and symmetric, i.e., $[Al/45/0/Al/0/45/Al]_T$, which gives rise to *Extension-Shearing* as well as *Bending-Twisting* coupling. By contrast, FML 1 and 5 contain orthotropic, cross-ply sub-laminates.

Similar observations have been made for profiles with different cross sections and for multi-layered laminates made only of fibre reinforced plastics [19]. Results from the experiments agree well with numerical simulations up to ultimate load [6, 16].

However, material failure, including delamination and progressive failure, was not assessed in the FE simulations, which explains the deeper deflections and longer post-buckling paths, beyond those of the experimental observations. Similar behaviour was observed for the flange response.

The aluminium layers were modelled as an elastic-plastic material with isotropic hardening, whereas glass-fibre composite plies were assumed to remain elastic up to failure [6, 15, 20]. The presence of ductile aluminium makes the post-buckling equilibrium curves flatter in comparison to the response of profiles made only from composite layers.

Buckling response also differs between the FML due to the presence of *Bending-Twisting* coupling in the *FRP* sub-laminates, which is known to reduce initial buckling strength and to induce mode changes in the post-buckling range [21]. The sequence in which the layers are stacked can be tailored in order to control stiffness coupling.

However, for FMLs, this effect has yet to be thoroughly quantified against practical designs. In the case of the buckling problem, the arrangement of plies must be ‘tailored’ with respect to their distance from the laminate mid-plane, since this influences the bending stiffness and in turn the buckling response. The literature describes strategies

for identifying laminate configurations with generic angle- and cross-ply combinations, including those with fully isotropic behaviour [12].

Although there is a perceived disadvantage due to lower buckling load for profiles made of hybrid FML, this is outweighed by a reduction in mass, which for the thin-walled columns investigated, reaches approximately 15%; a weight reduction which is an important factor in material selection for commercial aircraft applications [3].

5. Effect of mechanical coupling in Fibre Metal Laminates

The laminate constitutive equations, i.e. the relationship of the in-plane forces $\{N\}$ and moments $\{M\}$ to reference strain $\{\varepsilon\}$ and curvature $\{\kappa\}$ can be combined into one brief, well-known matrix equations [22, 23]

$$\begin{Bmatrix} \{N\} \\ \{M\} \end{Bmatrix} = \begin{bmatrix} [A] & [B] \\ [B] & [D] \end{bmatrix} \begin{Bmatrix} \{\varepsilon^{(0)}\} \\ \{\kappa\} \end{Bmatrix} \quad (1)$$

The equations (1) are expressed in terms of three laminate stiffness matrices, extensional $[A]$, coupling $[B]$, and bending $[D]$, which are functions of the geometry, material properties and stacking sequence of the individual plies [23]. The coupling behaviour is dependent on the form of the elements in each of these three stiffness matrices. Balanced and symmetric stacking sequences are adopted in standard FML designs, and generally possess *Bending-Twisting* coupling; often referred to as bending anisotropy in the literature.

These coupling effects are described in detail elsewhere [12, 24]. A Bending-Twisting coupled laminate, with the designation $\mathbf{A}_S\mathbf{B}_0\mathbf{D}_F$, signifies that the elements of the

extensional stiffness matrix $[A_s]$ are Specially orthotropic or Simple in nature, i.e. uncoupled, since

$$A_{16} = A_{26} = 0 \quad (2)$$

the bending-extension coupling matrix $[B_0]$ is null and all elements of the bending stiffness matrix $[D_F]$ are Finite, i.e. $D_{16}, D_{26} \neq 0$. The subscripts used can be further extended to indicate extensional isotropy, where \mathbf{A}_I replaces \mathbf{A}_S when

$$A_{16} = A_{26} = 0 \quad (3)$$

and

$$A_{66} = (A_{11} - A_{22})/2 \quad (4)$$

Also bending isotropy, can be indicated by replacing \mathbf{D}_S with \mathbf{D}_I , when

$$D_{ij} = A_{ij} H^2/12 \quad (5)$$

where H is a total laminate thickness corresponding to the total number of plies, n , of thickness t [12].

Tsai and Hahn introduced the useful concept of the laminate invariants U_i [25], which are calculated from the reduced stiffness matrix terms Q_{ij}

$$\begin{aligned}
U_1 &= (3Q_{11} + 3Q_{22} + 2Q_{12} + 4Q_{66})/8 \\
U_2 &= (Q_{11} - Q_{22})/2 \\
U_3 &= (Q_{11} + Q_{22} - 2Q_{12} - 4Q_{66})/8 \\
U_4 &= (Q_{11} + Q_{22} + 6Q_{12} - 4Q_{66})/8 \\
U_5 &= (Q_{11} + Q_{22} - 2Q_{12} + 4Q_{66})/8
\end{aligned} \tag{6}$$

and the reduced stiffness terms (on-axis moduli) are calculated from the material properties as follows

$$\begin{aligned}
Q_{11} &= E_1 / (1 - \nu_{12}\nu_{21}) \\
Q_{12} &= \nu_{12} E_2 / (1 - \nu_{12}\nu_{21}) \\
Q_{22} &= E_2 / (1 - \nu_{12}\nu_{21}) \\
Q_{66} &= G_{12}
\end{aligned} \tag{7}$$

Then the stiffness properties for the Equivalent Fully Isotropic Laminate can be obtained from the laminate invariants of Eqs. (6), expressed in terms of their isotropic material counterparts, with the assumption that $E_1 = E_2$, $\nu_{12} = \nu_{21}$, etc.

$$E_{Iso} = 2(1 + \nu_{Iso})G_{Iso} = U_1(1 - \nu_{Iso}^2) \tag{8}$$

with $\nu_{Iso} = U_4/U_1$ and $G_{Iso} = U_5$. The Young's modulus E_{Iso} , Poisson ratio ν_{Iso} , and shear modulus G_{Iso} , are the equivalent isotropic material properties of a composite laminate of thickness H , consisting of the total number of plies, n , of uniform thickness t . These relationships allow the equivalent isotropic stiffness properties of R-Glass and Carbon-epoxy materials compared to those of the metallic layers in hybrid materials, see Tables 2 and 3.

The equivalent isotropic stiffness properties for laminates with any number of plies can be expressed as follows

$$\begin{aligned}
A_{Iso} &= A_{11} = A_{22} = E_{Iso} H / (1 - \nu_{Iso}^2) = U_1 H \\
A_{12} &= \nu_{Iso} A_{11} \\
A_{66} &= U_5 H
\end{aligned} \tag{9}$$

The bending stiffness elements follow from Eq. (5) as

$$D_{Iso} = E_{Iso} H^3 (1 - \nu_{Iso}^2) / 12 = U_1 H^3 / 12 \tag{10}$$

Although the most commonly adopted method for achieving fully uncoupled laminates is the ubiquitous balanced and symmetric lay-up, non-symmetric laminate configurations are now known to dominate the design space of *Simple* (uncoupled), as well as *Bending-Twisting* coupled laminates [26, 27].

Applying these formulae to the FML designs considered, one can obtain the equivalent isotropic bending stiffness $D_{Iso} = 49\,391$ N.mm for FML 8 (monolithic aluminium) of Table 1, whereas for FML 9, $D_{Iso} = 39\,223$ N.mm for R-Glass/Epoxy (HexcelTM) when $H = 1.9$ mm.

For FML designs with Carbon/Epoxy 120EP-513/CF sub-laminates, $H = 1.86$ mm, and FML 8 gives $D_{Iso} = 46\,336$ N.mm, whereas for FML 9 $D_{Iso} = 41\,447$ N.mm. In all FML designs, $D_{ij} \neq A_{ij} H^2 / 12$ due to the lamination of more than one material.

The equivalent isotropic bending stiffness for monolithic aluminium used in the normalization of the buckling load results that follow.

The reduction in bending stiffness of FML below monolithic aluminium results in decreased buckling load, see Table 4, of up to approximately 25%. Additionally for a rectangular plate with aspect ratio $a/b = 3.75$, which corresponds to the aspect ratio the

channel section web, see Table 5, a similar drop is observed. These rectangular plate results correspond to a specific value on the Garland curves of Fig. 5, representing buckling factor results across a range of aspect ratios. Differences in the relative buckling strength between the channel section and the simply supported plate demonstrate the weak influence that the flanges have on web buckling.

A solid aluminium section profile and/or flat plate made from GFRP material designed as an equivalent fully isotropic laminate possesses higher buckling strength than those made from standard GLARE 3 (or FML 1 in Table 5), or GLARE 6A (or FML 10). However, the differences between the GLARE 3 and GLARE 6A are less than 5%.

It is obvious that replacing R-glass composite layers with carbon composite plies will give lower discrepancy in Young's moduli between both constituents and the equivalent bending stiffness differences will be less than for standard GLARE designs. The effect of such an exchange is visible in Table 6 where results are analogous to those from Table 5. The modified material properties are given in Table 3 [9, 20]. In first row, the notation 'AS60' represents an FML with an anti-symmetric Quasi-Homogenous Orthotropic sub-laminate $[\pm 45_2/-45_2/45_2/\pm 45_2]_T$ with NORTH PLY material of 60 gsm areal weight and ply thickness $t = 0.02$ mm. The drop in buckling load, when compared to monolithic aluminium channel or plate, is much lower than for R-Glass sub-laminates. The FML with an isotropic sub-laminate is approximately 10% lower, whilst the anti-symmetric Quasi-Homogenous Orthotropic sub-laminate is now only 4% lower. The improvement in buckling strength is therefore pronounced.

The relative difference between buckling loads for profiles made of different FML grades with carbon-epoxy layers looks similarly to the relationships observed in Fig. 5

for glass-epoxy, but the spacing between Garland curves are more pronounced, see Fig. 6, due to the increased influence of the higher modulus sub-laminates. It can be noticed that GLARE 6A (FML 10) has reducing buckling strength, i.e. 5.39%, 5.72% and 5.84% below the datum (Aluminium plate) for $a/b = 1, 2,$ and 3 respectively. This effect is caused by *Bending-Twisting* coupling in the carbon/epoxy sub-laminate [27].

These results demonstrate that carbon/epoxy has the potential to substantially increase buckling strength in FML designs. However, FML designs with isotropic or tailored sub-laminates require thin ply material technology to achieve the required stacking sequence configurations yet remain within the thickness constraint of standard FML designs.

6. Thin-ply technique

During the last decade evident progress has been made in the development of composite laminates using thinner plies. Compared to areal weights of standard composite materials of 300 gsm, thin-ply pre-pregs are commercially available down to as little as 15 gsm [28], with a corresponding thickness of 20 μm per single ply depending on the type of fibre. This generally increases the scope for laminate tailoring without affecting laminate thickness or weight.

The most important benefit of using thinner plies in a laminate design, for a constant laminate thickness, is the ability to use a larger number of ply orientations to achieve an optimal solution as the laminate design space is naturally extended. The second merit is that thin-ply composites may present some advantages due to positive size effects with respect to decreasing ply thickness. Although the use of thin-ply pre-pregs leads to

increase in manufacturing cost, the damage resistance properties against matrix cracking and delamination significantly improve. Despite identical stiffness for thin-ply and standard laminates compared, the tensile strength of the laminate using the thin-ply UD material is higher than that of the laminate using the standard UD material [7].

Composite laminates manufactured from thin-ply UD material are believed to have superior damage resistance properties compared to those from standard UD material. They are less susceptible to matrix crack accumulation than the standard laminate and to propagation of free-edge delamination. These observations have been verified experimentally [7].

Some pseudo-ductile effects were observed in the response of unidirectional interlayer hybrid composite materials comprising R-glass and a variety of thin carbon UD materials [20]. The materials considered for this hybrid design and examined in set of experiments were standard thickness R-glass/epoxy supplied by Hexcel, thin S3-glass/epoxy from North Thin Ply Technology and various thin carbon/epoxy from SK Chemicals and North Thin Ply Technology. The epoxy resin systems used in the prepregs were the aerospace grade 913 (Hexcel), Thin-Preg 120 EPHTg-402 (North Thin Ply Technology) and K50 (SK chemicals). The developed materials, under loads, exhibit a 60 GPa initial modulus, up to 970 MPa pseudo-yield stress and 1.44% pseudo-ductile strain.

In the available literature, which is not so abundant, there is some evidence that thin-ply material leads to a more uniform microstructure and improved on-axis compressive strength, hence nearly no damage is observed in thin ply material before failure. Some of these features result from the large number of sub-laminate repetitions. These special

material properties promise better predictability of behaviour from laminates manufactured using thin-ply technology.

Returning our attention to the buckling strength of FML profiles, standard GLARE architectures with carbon-epoxy sub-laminates are replaced with thin plies of 60 gsm areal weight to create $[Al/\pm 45_2/-45_2/45_2/\pm 45_2/Al/\pm 45_2/-45_2/45_2/\pm 45_2/Al]_T$ and $[Al/45_{12}/-45_{12}/Al/-45_{12}/45_{12}/Al]_T$ stacking sequences with the same overall sub-laminate thickness. Buckling loads for these thin-ply FML designs are compared again with monolithic aluminium plates in Fig. 7. The relationships are similar to those for standard carbon/epoxy layers, but the degradation in buckling load is significantly lower than for standard ply thickness, due to the elimination of *Bending-Twisting* coupling [30].

Hybrid laminates possess unusual stiffness relationships. For instance, sub-laminates may be designed to be fully isotropic with sufficient numbers of thin-ply layers, e.g. 24 layers: $[-45/90/0/45/0/45/90/45/-45/0/-45/90/-45/90/45/90/0/-45/0/45/0/45/-45/90]_T$, but the FML no longer satisfies Eq. (5). The hybridization renders the relationship proportional, rather than equal, i.e.: $D_{ij} \propto A_{ij}H^2/12$, even when all sub-laminates are individually isotropic in both extension and bending.

7. Lamination parameters for bending stiffness assessment of FML designs

Ply angle dependent lamination parameters may offer useful insight into the effects on buckling of different sub-laminate architectures, since they allow the bending stiffness terms to be expressed as linear variables within convenient bounds ($-1.0 \leq \xi_i \leq 1.0$), which are readily presented in graphical form to aid the design process [12]. Four

lamination parameters exist for each of the extension $(\xi_1 - \xi_4)$, coupling $(\xi_5 - \xi_8)$ and bending $(\xi_9 - \xi_{12})$ stiffness matrices. For the buckling assessment of laminated composite plates, only those for bending stiffness are of importance, given that the coupling stiffness matrix is assumed to be zero. Lamination parameters $(\xi_9 - \xi_{12})$ for FML are related to the elements of the bending stiffness matrix as follows

$$\begin{aligned} \begin{Bmatrix} D_{11} \\ D_{12} \\ D_{16} \\ D_{22} \\ D_{26} \\ D_{66} \end{Bmatrix} &= \frac{\zeta^{Al} H^3}{\zeta} \frac{1}{12} \begin{bmatrix} 1 & \xi_9^{Al} & \xi_{10}^{Al} & 0 & 0 \\ 0 & 0 & -\xi_{10}^{Al} & 1 & 0 \\ 0 & \xi_{11}^{Al}/2 & \xi_{12}^{Al} & 0 & 0 \\ 1 & -\xi_9^{Al} & \xi_{10}^{Al} & 0 & 0 \\ 0 & \xi_{11}^{Al}/2 & -\xi_{12}^{Al} & 0 & 0 \\ 0 & 0 & -\xi_{10}^{Al} & 0 & 1 \end{bmatrix} \begin{Bmatrix} U_1^{Al} \\ U_2^{Al} \\ U_3^{Al} \\ U_4^{Al} \\ U_5^{Al} \end{Bmatrix} + \\ \frac{\zeta^{FRP} H^3}{\zeta} \frac{1}{12} &\begin{bmatrix} 1 & \xi_9^{FRP} & \xi_{10}^{FRP} & 0 & 0 \\ 0 & 0 & -\xi_{10}^{FRP} & 1 & 0 \\ 0 & \xi_{11}^{FRP}/2 & \xi_{12}^{FRP} & 0 & 0 \\ 1 & -\xi_9^{FRP} & \xi_{10}^{FRP} & 0 & 0 \\ 0 & \xi_{11}^{FRP}/2 & -\xi_{12}^{FRP} & 0 & 0 \\ 0 & 0 & -\xi_{10}^{FRP} & 0 & 1 \end{bmatrix} \begin{Bmatrix} U_1^{FRP} \\ U_2^{FRP} \\ U_3^{FRP} \\ U_4^{FRP} \\ U_5^{FRP} \end{Bmatrix} \end{aligned} \quad (11)$$

where ζ^{Al} and ζ^{FRP} are non-dimensional bending stiffness parameters representing the contribution of the Aluminium (*Al*) and Fibre Reinforced Plastic (*FRP*) sub-laminates, with $\zeta = \zeta^{Al} + \zeta^{FRP}$. Assuming uniform ply thickness throughout, $\zeta = n^3$, where n is the number of plies in the laminate, or, in this case, to satisfy non-uniform ply thickness between *Al* (0.3 mm) and *FRP* (0.25 mm) layers, a suitable fraction (0.05 mm) that permits the build-up of (6 or 5) contiguous plies to achieve the required thicknesses. The laminate invariants U_i are given in Eq. (6), noting that these are different for Carbon/epoxy or Glass/epoxy. Hence the lamination parameters for hybrid designs cannot be assessed in the same way as standard fibre/epoxy material designs.

Nevertheless, some degree of assessment is possible through inference; based on standard fibre/epoxy laminate properties, since the Aluminium sub-laminate will always be represented by the lamination parameter point for an isotropic laminate, if the layers are symmetrically placed about the laminate mid-plane. Standard ply orientations ($\pm 45^\circ$, 0° and 90°) have been chosen specifically because they have most relevance to current design practice; this strategy also reduces the lamination parameter data to a 3-dimensional set, since the particular choice of angle ply, $\pm \theta = \pm 45^\circ$, then renders $\xi_{12} = 0$. The isotropic laminate corresponds to the coordinate $(\xi_9, \xi_{10}, \xi_{11}) = (0.0, 0.0, 0.0)$ in the lamination parameter design space.

GLARE 6A contains an angle-ply sub-laminate, which corresponds to the lamination parameter coordinate (0.0, -1.0, 0.553). The bending stiffness contributions of the ζ^{Al} and ζ^{FRP} are 68% and 32% respectively.

The bending stiffness contributions are dependent on non-dimensional parameters relating to the geometric distribution of each sub-laminate, and are defined as

$$\begin{aligned}\zeta_{+45}^{FRP} &= 4 \sum_{\theta=+45} (z_k^3 - z_{k-1}^3) / 12, \quad \zeta_{-45}^{FRP} = 4 \sum_{\theta=-45} (z_k^3 - z_{k-1}^3) / 12, \\ \zeta_0^{FRP} &= 4 \sum_{\theta=0} (z_k^3 - z_{k-1}^3) / 12, \quad \zeta_{90}^{FRP} = 4 \sum_{\theta=90} (z_k^3 - z_{k-1}^3) / 12\end{aligned}\tag{12}$$

where $\zeta^{FRP} = \zeta_{+45}^{FRP} + \zeta_{-45}^{FRP} + \zeta_0^{FRP} + \zeta_{90}^{FRP}$

Lamination parameters represent an angle ply dependent form of these non-dimensional parameters

$$\begin{aligned} \zeta_9^{FRP} &= \left\{ \zeta_{+45}^{FRP} \cos(2 \times 45^\circ) + \zeta_{-45}^{FRP} \cos(2 \times -45^\circ) + \zeta_0^{FRP} \cos(2 \times 0^\circ) + \zeta_{90}^{FRP} \cos(2 \times 90^\circ) \right\} / \zeta^{FRP} \\ \zeta_{10}^{FRP} &= \left\{ \zeta_{+45}^{FRP} \cos(4 \times 45^\circ) + \zeta_{-45}^{FRP} \cos(4 \times -45^\circ) + \zeta_0^{FRP} \cos(4 \times 0^\circ) + \zeta_{90}^{FRP} \cos(4 \times 90^\circ) \right\} / \zeta^{FRP} \end{aligned} \quad (13)$$

$$\zeta_{11}^{FRP} = \left\{ \zeta_{+45}^{FRP} \sin(2 \times 45^\circ) + \zeta_{-45}^{FRP} \sin(2 \times -45^\circ) + \zeta_0^{FRP} \sin(2 \times 0^\circ) + \zeta_{90}^{FRP} \sin(2 \times 90^\circ) \right\} / \zeta^{FRP}$$

By contrast, for isotropic layers (*Al*),

$$\zeta^{Al} = \zeta_{+45}^{Al} = \zeta_{-45}^{Al} = \zeta_0^{Al} = \zeta_{90}^{Al} \quad (14)$$

and given that *Al* can be considered as an *FRP* material with an infinite number of equally spaced fibre orientations, each with equal bending stiffness contribution,

$$\begin{aligned} \zeta_9^{Al} &\cong \zeta^{Al} \sum_{i=1}^{\infty} \cos(2\theta_{i\pi/\infty}) = \\ \zeta_{10}^{Al} &\cong \zeta^{Al} \sum_{i=1}^{\infty} \cos(4\theta_{i\pi/\infty}) = \\ \zeta_{11}^{Al} &\cong \zeta^{Al} \sum_{i=1}^{\infty} \sin(2\theta_{i\pi/\infty}) = 0 \end{aligned} \quad (15)$$

or, as in this case equal numbers of fibres in each of the four standard fibre orientations.

Additionally, the laminate invariants U_i of Eq. (6) for Aluminium lead to $U_2 = U_3 = 0$.

These simplifying effects reduce Eqn. (11) to the following form

$$\begin{Bmatrix} D_{11} \\ D_{12} \\ D_{16} \\ D_{22} \\ D_{26} \\ D_{66} \end{Bmatrix} = \frac{\zeta^{Al} H^3}{\zeta} \frac{1}{12} \begin{Bmatrix} U_1^{Al} \\ U_4^{Al} \\ 0 \\ U_1^{Al} \\ 0 \\ U_5^{Al} \end{Bmatrix} + \frac{\zeta^{FRP} H^3}{\zeta} \frac{1}{12} \begin{bmatrix} 1 & \zeta_9^{FRP} & \zeta_{10}^{FRP} & 0 & 0 \\ 0 & 0 & -\zeta_{10}^{FRP} & 1 & 0 \\ 0 & \zeta_{11}^{FRP}/2 & 0 & 0 & 0 \\ 1 & -\zeta_9^{FRP} & \zeta_{10}^{FRP} & 0 & 0 \\ 0 & \zeta_{11}^{FRP}/2 & 0 & 0 & 0 \\ 0 & 0 & -\zeta_{10}^{FRP} & 0 & 1 \end{bmatrix} \begin{Bmatrix} U_1^{FRP} \\ U_2^{FRP} \\ U_3^{FRP} \\ U_4^{FRP} \\ U_5^{FRP} \end{Bmatrix} \quad (16)$$

and for GLARE 6A, the lamination parameter for the *FRP* sub-laminate is

$(\xi_9, \xi_{10}, \xi_{11}) = (0.0, -1.0, 0.553)$. The D_{ij} for the two sub-laminates, and the resulting

FML, are given in Table 7.

8. Comparison with buckling results obtained from Carbon/Epoxy composite materials

For optimum design subject to buckling and/or strength constraints, ply angle dependent lamination parameters are often preferred, since these allow the stiffness terms to be expressed as linear variables within convenient bounds ($-1.0 \leq \xi_i \leq 1.0$). However, the optimized lamination parameters must then be matched to a corresponding laminate configuration within the feasible region. This inverse problem is often challenging, but is aided by graphical representations of the lamination parameter design spaces in which lamination parameter coordinates can be plotted. Buckling contour mapping can also be applied to these lamination design spaces, as illustrated in Fig. 8; here representing compression loaded infinitely long plates with simply supported edges.

Figure 8(a) indicates the feasible region of the 3-dimensional lamination parameter design space together with 3 cross-sections, taken on planes at $\xi_{11} = 0, 0.5$ and 0.6 to illustrate the variation in the buckling factor contours with increasing *Bending-Twisting* coupling.

Cross-ply laminates, which are commonly adopted as sub-laminates in FML design (e.g. GLARE 3) can be plotted in Fig. 8b. Note that whilst these have equal number of 0 and 90° plies, the bending contributions are not equal due to the different interface distances about the laminate mid-plane. By contrast, balanced plain weave sub-

laminates would possess equal bending stiffness contributions, with lamination parameter co-ordinates $(\xi_9, \xi_{10} = 0, 1)$. The isotropic laminate with equal bending stiffness contributions from 0, 90, 45 and -45° plies corresponds to $(\xi_9, \xi_{10} = 0, 0)$ and possesses the classical buckling load factor $k_{x,\infty} = 4.0$. Angle-ply sub-laminates with equal bending stiffness contributions from the +45 and -45° plies correspond to co-ordinates $(\xi_9, \xi_{10} = 0, -1)$, with buckling load factor $k_{x,\infty} = 5.05$.

Note that buckling loads are reduced whenever *Bending-Twisting* coupling is present, as is often the case in symmetric designs containing angle ply sub-laminates (e.g. GLARE 6A or 6B); the magnitude of the reduction increases with increasing *Bending-Twisting* coupling, in proportion to the corresponding lamination parameter $(\xi_{11} \geq 0)$. This is of course dependent on the volume fraction and relative position, from the laminate mid-plane, of each of the two material phases, hence the influence of *Bending-Twisting* coupling in FML is substantially reduced.

By contrast, *FRP* material is significantly affected by the presence of *Bending-Twisting* coupling. This is illustrated in the cross-sectional planes of Figs. 8c and 8d, which bound the *FRP* sub-laminate $(0.5 \leq \xi_{11} \leq 0.6)$ contained within GLARE 6A. This sub-laminate clearly has a significantly lower compression buckling strength $(4.13 < k_{x,\infty} < 4.42)$ than the angle-ply laminate $(k_{x,\infty} = 5.05)$ in which the *Bending-Twisting* coupling has been eliminated through laminate tailoring.

These results demonstrate that the comparatively higher compression buckling strength of an angle-ply *FRP* sub-laminate does little to influence the buckling strength of the FML, even if the presence of *Bending-Twisting* coupling is ignored.

Glass/Epoxy sub-laminates provide a relatively insignificant contribution to bending stiffness and despite the increased stiffness of Carbon/Epoxy, including the elimination of the detrimental effects of *Bending-Twisting* coupling within the *FRP* sub-laminate, the high volume fraction of the metal layers in traditional FML severely limits the extent to which buckling strength can be improved by the use of laminate tailoring. In all cases, the FML resulted in a lower buckling factor than the monolithic Aluminium datum. However it should be noted that these comparisons do not consider specific buckling strength (k_x/ρ), taking into account the reduced density (ρ) of the hybrid material.

9. Conclusions

The aim of the work was a comparison of the application of ‘classical’ Fibre Reinforce Plastic (*FRP*) layers versus ‘thin-ply technology’ designs, applied to Fibre-Metal-Laminate (FML) plate structures. These included thin-walled Channel cross-section profiles adopting a 3/2 FML lay-up design, made of 3 aluminium layers. Comparisons were made between composite sub-laminates with different materials, i.e. ‘classical’ Glass Fibre Reinforce Plastic (*GFRP*) and thin-ply Carbon Fibre Reinforce Plastic (*CFRP*). Different stacking sequences were also considered. Comparisons of uni-axial compression buckling strength were obtained by various methods, among them a semi-analytical method, a finite element method and experimental investigations.

The hybridization of materials in multi-layered structures for fatigue property improvement leads to an inevitable decrease in the buckling load capacity, but this effect is off-set to some extent by a measurable weight reduction. Multi-layered *FRP* materials are very effective for meeting tailored structural property requirements

through appropriate modification of mechanical stiffness properties, which govern the laminate response. Controlling the bending stiffness through appropriate laminate tailoring strategies, and material and ply thickness selection has been shown to give improvements in the compressive buckling load capacity for FML short columns of open cross-section. This was achieved through the introduction thin-ply technology in the *FRP* sub-laminates to replace traditional *GFRP* or *CFRP* layers. Improvements in buckling strength of FML designs have been demonstrated through the use of lamination parameter design spaces onto which buckling factor contours have been mapped. This technique provides a very useful tool for assessment and prediction of new hybrid FML panel designs.

Acknowledgements

This study is supported by the Ministry of Science and Higher Education of Poland - National Science Centre Grant No UMO-2012/07/B/ST8/04093.

The second author wishes to acknowledge the valuable discussions with Professor Sérgio Frascino Müller de Almeida, which have indirectly contributed to this study, and for the financial support of the Newton Research Collaboration Programme - NRCP1516/4/50.

References

1. Vlot A. Gunnik J.W., Fiber Metal Laminates, An Introduction. Springer Science+Business Media B.V., 2001.

2. Alderliesten R.C., Designing for damage tolerance in aerospace: A hybrid material technology, *Materials and Design*, 2015;66:421-428.
3. Vermeeren C. (ed.), *Around GLARE, A new aircraft material in context*. Kluwer Academic Publishers. 2004.
4. Verolme J.L. The initial buckling behavior of flat and curved fiber metal laminate panels. Delft University of Technology, Faculty of Aero. Eng, Report LR-785, 1995.
5. Alderliesten R., On the Development of Hybrid Material Concepts for Aircraft Structures, *Recent Patents on Engineering*, 2009;3:25-38.
6. Mania R.J., Kolakowski Z., Bienias J., Jakubczak P., Majerski K., Comparative study of FML profiles buckling and postbuckling behaviour under axial loading, *Composite Structures*, 2015;134:216-225.
7. Yokozeki T., Aoki Y., Ogasawara T. Experimental characterization of strength and damage resistance properties of thin-ply carbon fiber/toughened epoxy laminates, *Composite Structures*, 2008;82:382-389.
8. De Jong, T.W., Kroon, E., Sinke, J. Formability, In: Vlot, A., Gunnink, J.W. (Eds.), *Fibre Metal Laminates - an introduction*, Kluwer Academic Publishers, Dordrecht, The Netherlands, 2001.
9. Amacher R., Cugnoni J., Botsis J., Sorensen L., Smith W., Dransfeld C., Thin ply composites: Experimental characterization and modelling of size-effects, *Comp. Science and Technology*, 2014;101:121-132.
10. Sihm S., Kim R. Y., Kawabe K., Tsai S.W., Experimental studies of thin-ply laminated composites, *Composites Science and Technology*, 2007;67:996-1008.

11. Bieniaś J., Fibre Metal Laminates - some aspects of manufacturing process, structure and selected properties, *Compos. Theory Pract.*, 2011;11:39-43.
12. York C.B., Unified approach to the characterization of coupled composite laminates: benchmark configurations and special cases. *Journal of Aerospace Engineering*, 2010;23:219-242.
13. Kamocka M., Zglinicki M., Mania R.J., Multi-method approach for FML mechanical properties prediction, *Composites Part B Eng.*, 2016;91:135-143.
14. Kolakowski Z., Mania J.R., Semi-analytical method versus the FEM for analysis of the local post-buckling. *Composite Structures*, 2013;97:99-106.
15. Banat D., Kolakowski Z., Mania R.J., Investigations of FML profile buckling and post-buckling behaviour under axial compression, *Thin-Walled Structures*, 2016;107:335-344.
16. Mania R.J., Banat D., Modelling of boundary conditions in Fiber Metal Laminate buckling investigations, in: Mania R.J. (Ed.), *Statics, Dyn. and Stab. of Struct., Buckling of Plate Struct. in Anal. and Numer. Exp. Investig.*, Vol. 4, Lodz University of Technology, Series of Monographs, 2016: pp. 49-66.
17. Singer J., Arbocz J., Weller T., *Buckling Experiments Experimental Methods in Buckling of Thin-Walled Structures*. Willey, 1998.
18. Paszkiewicz M., Kubiak T., Selected problems concerning determination of the buckling load of channel section beams and columns, *Thin-Walled Structures*, 2015;93:112-121.
19. Kubiak T., Mania R.J., Hybrid versus FR laminate channel section columns – Buckling and postbuckling behaviour, *Composite Structures*, 2016;154:142-149.

20. Czél G., Jalalvand M., Wisnom M.R., Design and characterisation of advanced pseudo-ductile unidirectional thin-ply carbon/epoxy-glass/epoxy hybrid composites, *Composite Structures*, 2016;143:362-370.
21. York, C. B. On Extension-Shearing coupled laminates. *Composite Structures*, 2015;120:472-482.
22. Reddy J.N., *Mechanics of laminated composite plates and shells, theory and analysis*, CRC Press, 2004.
23. Jones, R.M., *Mechanics of Composite Materials*, Taylor & Francis, London, 1999.
24. ESDU - Stiffnesses of laminated plates. Engineering sciences data unit, Item no. 94003; 1994
25. Tsai S., Hahn H.T., *Introduction to Composite Materials*, Technomic Pub. Comp., 1980.
26. York, C. B. Characterization of non-symmetric forms of fully orthotropic laminates. *J. Aircraft* 2009;46:1114-1125.
27. York, C. B. On Bending-Twisting coupled laminates. *Composite Structures*, 2016; Under review.
28. North Thin Ply Technology, Conference Showcase, Reinforced Plastics, vol. 60, No 1, January/February 2016, pp. 28-29.
29. Mania R.J., York C.B. Buckling strength of FML profiles of 'classic' versus thin-ply design, in: Mania R.J. (Ed.), *Statics, Dynamics and Stability of Struct.*, *Research Advances in Applied Mechanics*, vol. 6, Lodz University of Technology, Series of Monographs, 2016: pp. 88-110.

30. York C. B., Influence of bending-twisting coupling on compression and shear buckling strength (Keynote), Proc. of Stability of Structures 14th Symposium, Zakopane, Poland, 2015, pp. 23-24.

Figures

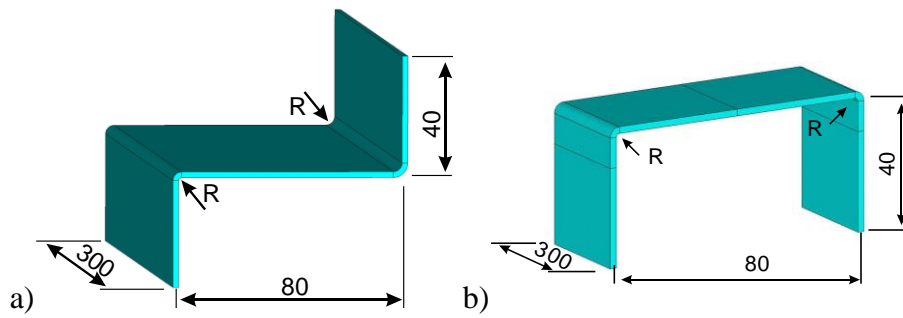


Fig. 1. Overall dimensions of Z-shape (a) and channel section (b).

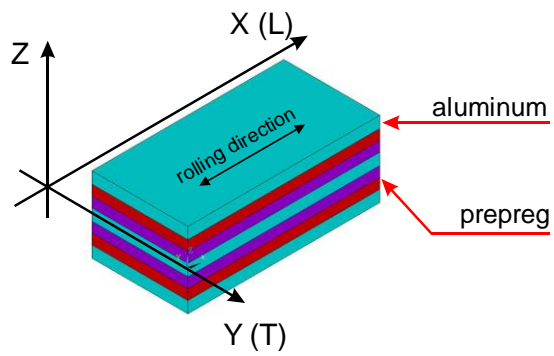


Fig. 2. 3/2 FML layup configuration.

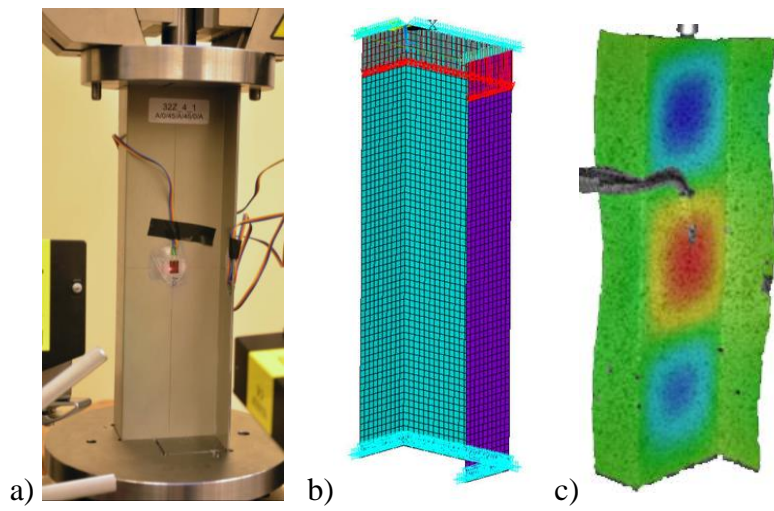


Fig. 3. FML channel section, illustrating: (a) Experimental test rig; (b) FEM model and; (c) DIC buckling mode.

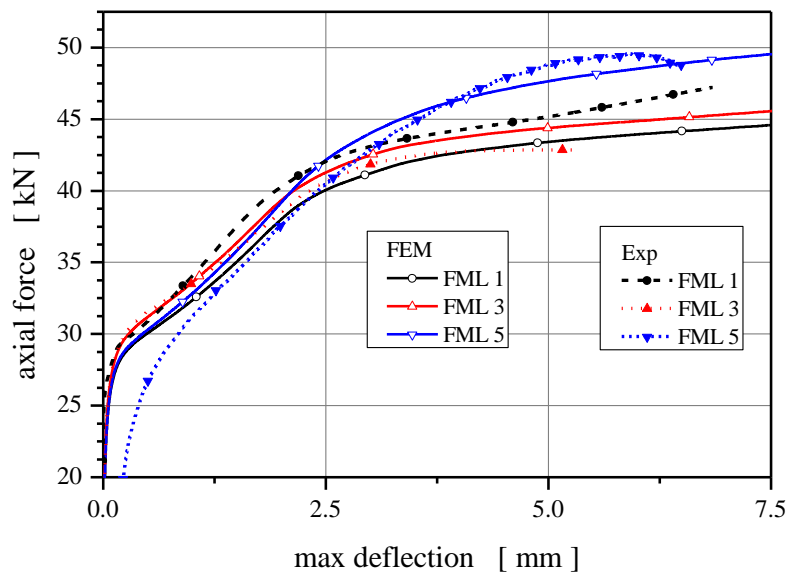


Fig. 4. Load-deflection curves for channel section post-buckling response.

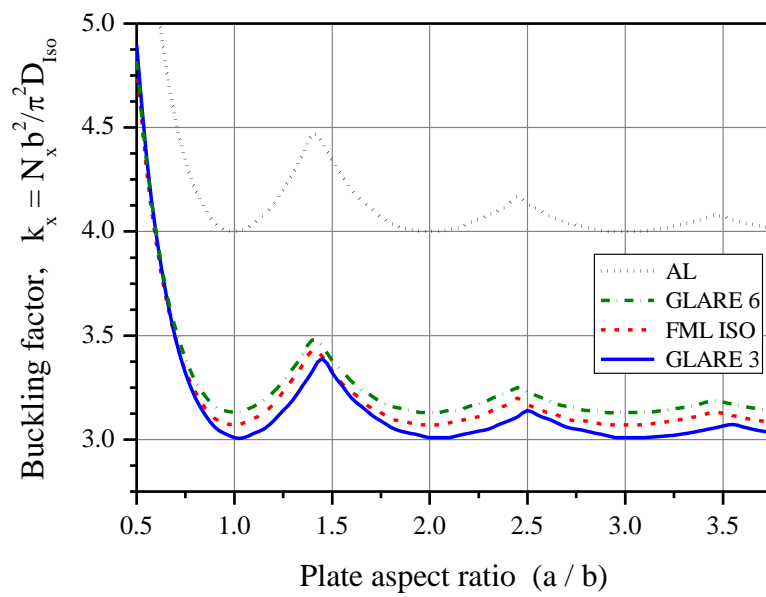


Fig. 5. Compression buckling factor curves for Standard FML designs with aluminium and R-Glass/Epoxy: GLARE 3 [Al/0/90/Al/90/0/Al]_T and GLARE 6A [Al/45/-45/Al/-45/45/Al]_T.

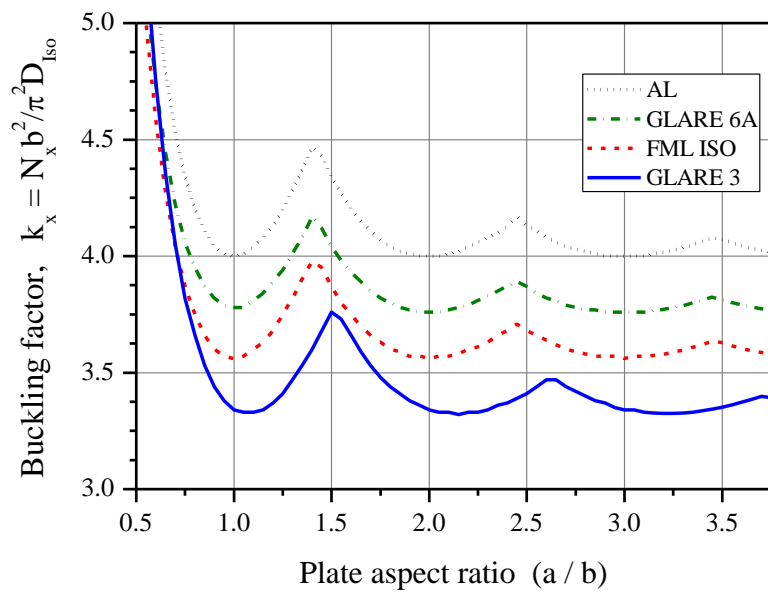


Fig. 6. Compression buckling factor curves for standard FML designs with aluminium and carbon/epoxy: (a) GLARE 3 [Al/0/90/Al/90/0/Al]_T and; (b) GLARE 6A [Al/45/-45/Al/-45/45/Al]_T. Al and FML_{ISO} represent a monolithic aluminium design and a standard FML design but with an isotropic carbon/epoxy sub-laminate.

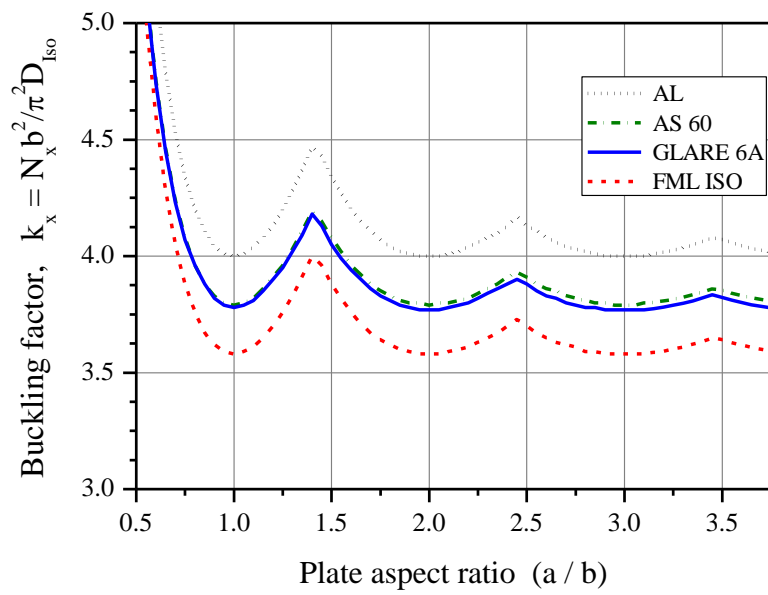
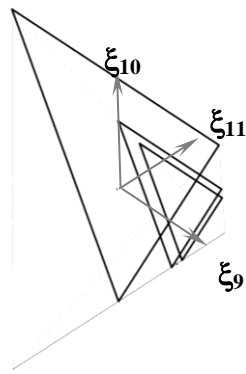


Fig. 7. Compression buckling factor curves for NORTH PLY FML designs with aluminium and Carbon/Epoxy (60gsm): GLARE 3 [Al/ $\pm 45_2$ / $-45_2/45_2/\pm 45_2$ /Al/ $\pm 45_2$ / $-45_2/45_2/\pm 45_2$ /Al]_T and GLARE 6A [Al/ 45_{12} / -45_{12} /Al/ $-45_{12}/45_{12}$ /Al]_T.



(a)

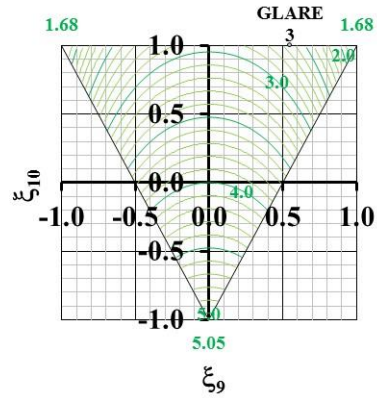
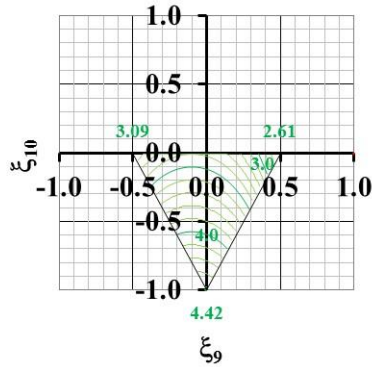
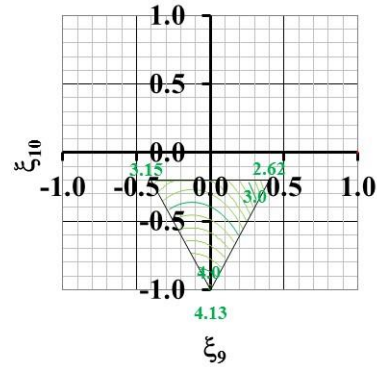
(b) $\xi_{11} = 0$ (c) $\xi_{11} = 0.5$ (d) $\xi_{11} = 0.6$

Fig. 8. The 3-dimensional lamination parameter design space illustrating (a) cross-sectional planes onto which compression buckling contours ($k_{x,\infty}$) are mapped for infinitely long plates with simply supported edges, at (b) $\xi_{11} = 0.0$ on which the *Al* sub-laminate is located, (c) $\xi_{11} = 0.5$ and; (d) $\xi_{11} = 0.4$, between which the *FRP* sub-laminate corresponding to GLARE 6A is located, i.e. $(\xi_9, \xi_{10}, \xi_{11}) = (0, -1, 0.553)$.

Figure Captions

Fig. 1. Overall dimensions of Z-shape (a) and channel section (b).

Fig. 2. 3/2 FML layup configuration.

Fig. 3. FML columns: (a) Experimental test rig; (b) FEM model and; (c) DIC buckling mode.

Fig. 4. Load-deflection curves for channel section post-buckling response.

Fig. 5. Compression buckling factor curves for Standard FML designs with aluminium and R-Glass/Epoxy: GLARE 3 $[Al/0/90/Al/90/0/Al]_T$ and GLARE 6A $[Al/45/-45/Al/-45/45/Al]_T$.

Fig. 6. Compression buckling factor curves for standard FML designs with aluminium and carbon/epoxy: (a) GLARE 3 $[Al/0/90/Al/90/0/Al]_T$ and; (b) GLARE 6A $[Al/45/-45/Al/-45/45/Al]_T$. Al and FML_{ISO} represent a monolithic aluminium design and a standard FML design but with an isotropic carbon/epoxy sub-laminate.

Fig. 7. Compression buckling factor curves for NORTH PLY FML designs with aluminium and Carbon/Epoxy (60gsm): GLARE 3 $[Al/\pm 45_2/-45_2/45_2/\pm 45_2/Al/\pm 45_2/-45_2/45_2/\pm 45_2/Al]_T$ and GLARE 6A $[Al/45_{12}/-45_{12}/Al/-45_{12}/45_{12}/Al]_T$.

Fig. 8. The 3-dimensional lamination parameter design space illustrating (a) cross-sectional planes onto which compression buckling contours ($k_{x,\infty}$) are mapped for infinitely long plates with simply supported edges, at (b) $\xi_{11} = 0.0$ on which the Al sub-

laminate is located, (c) $\xi_{11} = 0.5$ and; (d) $\xi_{11} = 0.4$, between which the *FRP* sub-laminate corresponding to GLARE 6A is located, i.e. $(\xi_9, \xi_{10}, \xi_{11}) = (0, -1, 0.553)$.

Tables

Table 1. Considered stacking sequences.

FML [GLARE]	Lay-up
1 [3]	A1/0/90/A1/90/0/A1
2	A1/90/0/A1/0/90/A1
3	A1/45/0/A1/0/45/A1
4	A1/0/45/A1/45/0/A1
5 [2A]	A1/0/0/A1/0/0/A1
6	A1/25/0/A1/0/25/A1
7	A1/0/25/A1/25/0/A1
8	A1/A1/A1/A1/A1/A1
9	A1/Iso/Iso/A1/Iso/Iso/A1
10 [6A]	A1/45/-45/A1/-45/45/A1

Table 2. Material properties for aluminium.

Material properties		Aluminium 2024-T3
Compressive moduli	E_1	77.00 GPa
(very small orthotropy for yield limit)	E_2	77.00 GPa
Shear modulus	G_{12}	28.95 GPa
Poison's ratio	ν_{12}	0.33

Table 3. Material properties for R-Glass/Epoxy and Carbon/Epoxy composite and equivalent isotropic properties.

Material properties		R-Glass/Epoxy (Hexcel™)	Carbon/Epoxy 120EP- 513/CF
Compressive moduli	E_1 (E_{Iso})	53.90 GPa (27.034 GPa)	136.1 GPa (51.712 GPa)
	E_2	14.92 GPa	7.01 GPa
	G_{12}	5.49 GPa (10.36 GPa)	4.661 GPa (19.868 GPa)
Shear modulus	(G_{Iso})		
Poisson's ratio	ν_{12} (ν_{Iso})	0.28 (0.3)	0.274 (0.3)

Table 4. Buckling loads of FML channel section columns.

FML No	Lay-up	Buckling force		
		exp [kN]	FEM [kN]	ANM Koiter [kN]
1	Al/0/90/Al/90/0/Al	31.434	30.189	28.568
2	Al/90/0/Al/0/90/Al	-	29.871	28.408
3	Al/45/0/Al/0/45/Al	32.634	31.399	29.876
4	Al/0/45/Al/45/0/Al	-	30.588	29.015
5	Al/0/0/Al/0/0/Al	29.836	30.310	28.630
6	Al/25/0/Al/0/25/Al	-	30.745	29.334
7	Al/0/25/Al/25/0/Al	29.856	30.977	28.859
8	Al/Al/Al/Al/Al/Al/Al	-	40.472	38.510
9	Al/Al/Al/Al/Al/Al/Al	-	30.805	31.380
10	Al/45/-45/Al/-45/45/Al	-	31.752	30.208

Table 5. Buckling comparisons between channel section buckling load and plate buckling factor, with matching web and plate aspect ratio ($a/b = 3.75$) for standard GFRP material or GLARE. Overall FML thickness $H = 1.9$ mm.

FML No	Buckling Load - Channel (kN)*	Relative Buckling strength	Buckling factor - Plate (k_x)	Relative Buckling strength
1	28.258	-22.5%	3.03	-24.5%
5	28.346	-22.2%	3.04	-24.3%
8	36.439	0.0%	4.02	0.0%
10	29.818	-18.2%	3.14	-21.8%

Table 6. Buckling comparisons between Channel section buckling load and plate buckling factor, with matching web and plate aspect ratio ($a/b = 3.75$) for NORTH PLY CFRP material. Overall FML thickness $H = 1.86$ mm.

FML	Buckling Load - Channel (kN)*	Relative Buckling strength	Buckling factor - Plate (k_x)	Relative Buckling strength
AS60	33.069	-3.3%	3.81	-5.2%
8	34.189	0.0%	4.02	0.0%
9	30.719	-10.1%	3.59	-10.6%
10	32.806	-4.0%	3.78	-5.9%

Table 7. Comparison of relative bending stiffness between *GFRP* and *Al* sub-laminates for GLARE 6A.

	D_{11}	D_{12}	D_{16}	D_{22}	D_{26}	D_{66}
<i>FRP</i>	4,508	2,523	982	4,508	982	2,754
<i>Al</i>	33,765	11,142	0	33,765	0	11,311
FML	38,273	13,665	982	38,273	982	14,065